Cosmic microwave background signatures from current-carrying cosmic strings

I. Yu. Rybak,[1,2,3,*] C. J. A. P. Martins,[2,3,†] Patrick Peter,[4,5,‡] and E. P. S. Shellard[5,§]

[1]*CAPA and Departamento de Física Teórica, Universidad de Zaragoza, Pedro Cerbuna, 12, 50009 Zaragoza, Spain*

[2]*Centro de Astrofísica da Universidade do Porto, Rua das Estrelas, 4150-762 Porto, Portugal*

[3]*Instituto de Astrofísica e Ciências do Espaço, CAUP, Rua das Estrelas, 4150-762 Porto, Portugal*

[4]*GReCO—Institut d'Astrophysique de Paris, CNRS and Sorbonne Université, UMR 7095 98 bis boulevard Arago, 75014 Paris, France*

[5]*Centre for Theoretical Cosmology, Department of Applied Mathematics and Theoretical Physics, University of Cambridge, Wilberforce Road, Cambridge CB3 0WA, United Kingdom*

(Received 26 March 2024; accepted 15 June 2024; published 22 July 2024)

We continue our studies of the evolution and cosmological consequences of current-carrying cosmic string networks, described by a charge-velocity-dependent one scale (CVOS) model. We present a detailed calculation of the effects of these networks on the cosmic microwave background (CMB), in the context of this model, and specifically discuss how such current-carrying strings may be distinguished from their uncharged (Nambu-Goto) counterparts by current or forthcoming CMB data. We find that, under the CVOS hypothesis, the constraints on current-carrying strings should not differ much from those of their structureless counterparts in that the impact on the CMB can at most be reduced by a factor of ∼25%. Nevertheless, the presence of a current and charge affects the distribution of power among scalar, vector and tensor modes, and also its distribution between small and large scales. It should therefore be possible for future high-sensitivity CMB temperature and polarization experiments to distinguish between the two types of strings.

DOI: 10.1103/PhysRevD.110.023534

I. INTRODUCTION

Cosmic strings provide a valuable probe for investigating possible high-energy scenarios in the early Universe [1–4]. To accurately constrain high-energy physics using cosmic strings, it is crucial to understand the evolution of their networks in quantitative detail. In particular, this requires a comprehensive understanding of all possible additional degrees of freedom and structures, such as long-lasting currents [5–10], often dubbed superconducting—a nomenclature we prefer not to use here as it often refers to long-range electromagnetic effects—and Y-junctions [11,12], each of which can introduce deviations from the conventional cosmic string evolution paradigm [13–17]. Naturally, any such deviations can also impact their observational predictions and the constraints obtained based on them [18–23].

To gain insights into the evolution of these one-dimensional topological defects, it is more common to appeal to field theory simulations [24–26]. Another approach involves simulating cosmic strings as infinitely thin entities governed by the Nambu-Goto action [27–29]. However, these approaches have, so far, not successfully achieved full-scale simulations of current-carrying string networks, although efforts toward this goal are presently ongoing. Thus, to address the evolution of a network of such strings, we make use of the thermodynamical approach known as the charge-velocity-dependent one-scale (CVOS) model [30–32], which extends the original VOS model developed for ordinary cosmic strings in Refs. [33,34].

A particularly sensitive and well-established probe to assess the presence of cosmic strings is the study of cosmic microwave background (CMB) anisotropies [35–37], which rely on linear physics, to which one may also add spectral distortions [38–40] and lensing [41–43]. In particular, anisotropies generated by ordinary cosmic strings, whether they are estimated from field theory, Nambu-Goto simulations or analytical approaches, yield similar predictions [44,45]; see however Ref. [46] for detailed comparison and possible discrepancies between different methods.

In the absence of simulations depicting the evolution of current-carrying string networks, albeit recent advancements in simulating individual superconducting strings [47–50], we proceed to expand upon the CMBACT code [51]. We employ

*Contact author: irybak@unizar.es
†Contact author: Carlos.Martins@astro.up.pt
‡Contact author: patrick.peter@iap.fr
§Contact author: E.P.S.Shellard@damtp.cam.ac.uk

the CVOS model to compute the CMB anisotropies resulting from these networks, while considering various assumptions regarding the model's phenomenological parameters. Previous work [32] has shown that, depending on these model parameters and also the cosmological epoch, these networks may find themselves in frozen regimes (where the charge and current dominate) or in standard scaling solutions (with the charge and current disappearing). Other things being equal, the former scenario may have some likelihood of happening in the radiation era, while the latter is strongly indicated in the matter era. Once accurate simulations of these networks become available one may expect to measure these parameters directly from simulations, thereby determining which specific scenarios are realized in practice, but for the moment we scan the parameter space, and illustrate the results by considering representative examples of the various possible scenarios and exploring the consequences of each of them. Our results reveal distinctive CMB features associated with the presence of charges and currents, which have the potential to differentiate between general current-carrying and ordinary string networks.

Throughout this work we use the following cosmological (Planck best fit) parameters [52]: $\Omega_{\rm b0}h^2 = 0.0224$, $\Omega_{\rm m0}h^2 = 0.1424$, $H_0 = 100h\ \mathrm{km\cdot s^{-1}\cdot Mpc^{-1}}$, where $h = 0.674$. For definiteness, and in agreement with the currently accepted constraints, when a fiducial value of the string tension is necessary for a quantitative calculation, we set it to the value $G\mu_0 = 10^{-7}$ [53].

II. CVOS FORMALISM AND LINEAR MODEL

Current-carrying string networks can be described by the CVOS model originally developed in Ref. [30]. We briefly review its salient features in this section, referring the reader to the original work for additional technicalities and discussion.

This model contains four key macroscopic parameters, which are

(i) the root-mean-square (RMS) velocity v of the string network, that is the average magnitude of string velocities using a convenient statistical measure,

(ii) the characteristic length $\xi_{\rm C}$ of the network, which represents the averaged distance between cosmic strings and can be related to the energy density of strings, excluding charge and current, as

$$\rho_0 = \frac{\mu_0}{\xi_{\rm C}^2},$$

where the constant μ_0 is the tension or mass per unit length of bare strings,

(iii) the charge amplitude

$$Y = \frac{1}{2}(Q^2 + J^2),$$

with Q and J respectively the timelike and spacelike components of the averaged four-current, and

(iv) The chirality

$$K = Q^2 - J^2,$$

which determines whether the average string network possesses a globally timelike $K > 0$, spacelike $K < 0$ or lightlike $K = 0$ (chiral) current. It can be expressed as an averaged Lorentz-invariant two-current amplitude.

Another important ingredient that is required in the CVOS model for a current-carrying cosmic string network is an equation of state. The Witten model, considered at first in Ref. [5], is characterized by the following averaged equation of state [54]

$$\begin{cases} F_{\rm mag}(K) = 1 - \frac{1}{2}\frac{K}{1-\alpha K} & \text{for } K \le 0, \\ F_{\rm elec}(K) = 1 + \frac{\ln(1-\alpha K)}{2\alpha} & \text{for } K \ge 0, \end{cases} \tag{1}$$

where the dimensionless parameter

$$\alpha = \left(\frac{m_{\rm H}}{m_\sigma}\right)^2$$

is the square ratio of the mass of the string-forming Higgs field $m_{\rm H}$ with the vacuum mass of the current-generating condensate m_σ; this depends on the particular characteristics of the symmetry breaking process which resulted in the formation of current-carrying cosmic strings. In all of these scenarios, we have $1 < \alpha < \infty$ and, while many cases of particle physics relevance have $\alpha \gg 1$ holds, the strongest backreaction occurs with $\alpha \approx \mathcal{O}(1)$.

We are interested in cosmic string networks evolving in an expanding universe background defined by the homogeneous and isotropic Friedman-Lemaître-Robertson-Walker (FLRW) metric

$$\mathrm{d}s^2 = a(\tau)^2(\mathrm{d}\tau^2 - \mathrm{d}\boldsymbol{x}^2), \tag{2}$$

where $a(\tau)$ is the scale factor, τ is conformal time and $\boldsymbol{x}$ represents spatial components. The study of the CVOS model with the equation of state (1) on a FLRW background was carried out in Ref. [32], The results therein suggest that for most physically justified scenarios, in particular when $K(0) \approx 0$, and if one is interested in a macroscopic description, the Witten model is identical or dynamically driven to the linear model studied in Ref. [31]. Thus, in what follows we focus our attention on the linear version of the CVOS model whose equations of motion read

$$\begin{cases} \frac{d\xi_C}{d\tau} = \frac{\xi_C v^2}{1+Y}\frac{\dot{a}}{a} + \frac{cv}{2} + \frac{Y}{1+Y}vk(v), \\ \frac{dv}{d\tau} = \frac{(1-v^2)}{1+Y}\left[\frac{k(v)(1-Y)}{\xi_C} - 2v\frac{\dot{a}}{a}\right], \\ \frac{dY}{d\tau} = 2Y\left[\frac{vk(v)}{\xi_C} - \frac{\dot{a}}{a}\right] - \frac{Y}{\xi_C}A(Y), \end{cases} \tag{3}$$

with the salient point that the chirality evolution equation

$$\frac{dK}{d\tau} = 2K\left[\frac{vk(v)}{\xi_C} - \frac{\dot{a}}{a}\right] - \frac{K}{\xi_C}A(Y), \tag{4}$$

decouples from that of the other thermodynamical variables where we employed the comoving characteristic length $\xi = \xi_C a$ for convenience. When numerically solving Eqs. (3), we set the chopping efficiency to its Nambu-Goto (NG) value, i.e., $c \to c_{NG} \simeq 0.23$ [except for our so-called Model "(a)", to be defined in what follows, which has $c \to 0.5$], and the momentum parameter $k(v)$ is assumed to be, following [34]

$$k(v) \to k_{NG}(v) = \frac{2\sqrt{2}}{\pi}\frac{1-8v^6}{1+8v^6}(1-v^2)(1+2\sqrt{2}v^3). \tag{5}$$

Note that here we are making the assumption that the fact that $k(v)$ only depends explicitly on velocity, which is valid in the structureless case, still applies on the presence of charge and current (or some combination thereof, such as chirality). In other words, the assumption is that there is no explicit dependence of these additional degrees of freedom. There is clearly an indirect dependence, since the presence of charge or current will affect the velocity. Testing this assumption will require numerical simulations, and is therefore left for future work.

Although this reproduces the features measured in the string network simulations, it is often sufficient, in order to describe the scaling solution, to give $k(v)$ a constant value, i.e. $k(v) \to k_{sc} = k(v_{SC})$ since in particular the function (5) presents a plateau in the relevant regime in which the solutions are obtained. This is the choice we made in particular for our special cases, denoted (a), (b), (c) and (d) below, in agreement with Ref. [31]. It should be noted at this point that the so-called *chiral limit* $K \to 0$, corresponding to the case for which the charge and the current are equal, is an attractor for this system. As a result, we shall restrict attention to this case only, and replace the full system by a single parameter Y_{SC} in the forthcoming CMB analysis.

The charge leakage efficiency A is another phenomenological parameter, not derivable from the microscopic equations of motion. It is introduced in order to take into account all the microscopic effects, such as large local curvatures, through which the charge and current initially flowing along the strings may escape the long string network [55]. Moreover, both timelike and spacelike currents are seen to saturate somewhat for critical values, so the leakage A is expected to diverge when Y reaches a critical value, denoted Y_{cr} [56]. Various functional forms for $A(Y)$ can be used, as was suggested in Ref. [32]; in what follows, we will assume

$$A(Y) = \frac{A_c}{1 - e^{-(Y-Y_{cr})^2}}, \tag{6}$$

where A_c and

$$Y_{cr} = \frac{2}{3\alpha} = \frac{2m_\sigma^2}{3m_H^2} \tag{7}$$

are constant parameters which depend on the properties of the original field theory model. We can note at this stage that with $\alpha \gg 1$, the critical current is expected to be rather small in physically relevant cosmologies, thereby once again justifying the use of the linear model. The system (3) can be solved numerically using the leakage function (6), resulting examples begin shown in Fig. 1, superimposed with the analytic one-parameter expansion to which we now turn.

III. ONE-PARAMETER APPROXIMATION FOR CHARGE AND CURRENT EVOLUTION

The evolution of the model described by Eqs. (3) has been studied in detail in Refs. [31,32]. There it was shown that, for $a(\tau) \propto \tau^n$, a nonvanishing charge leakage leads to a scaling behavior, i.e.,

$$L_C = \zeta_{SC}\tau, \qquad \xi_C = \epsilon_{SC}\tau, \qquad v = v_{SC}, \qquad Y = Y_{SC}, \tag{8}$$

where the "sc" subscripts refer to the scaling values, which are constants. The energy density of the string network is given by

$$\rho = \frac{\mu_0}{a^2 L_C^2}, \quad \text{with} \quad \xi_C^2 = (1+Y)L_C^2 \tag{9}$$

(see Ref. [30] for details).

Throughout the radiation dominated epoch, depending on initial conditions, the CVOS model predicts two possible evolution regimes, namely the standard Nambu-Goto evolution with trivial (vanishing) charge $Y_{SC} = 0$, and a current-carrying (or charged) regime with $Y_{SC} \neq 0$. This is to be contrasted with the matter dominated epoch (and any faster expansion rates), which has only one possible regime, which is a standard Nambu-Goto evolution with $Y_{SC} = 0$. Thus, the evolution of the system (3) in an expanding universe is determined only by a charge amplitude Y_{SC} in the radiation epoch.

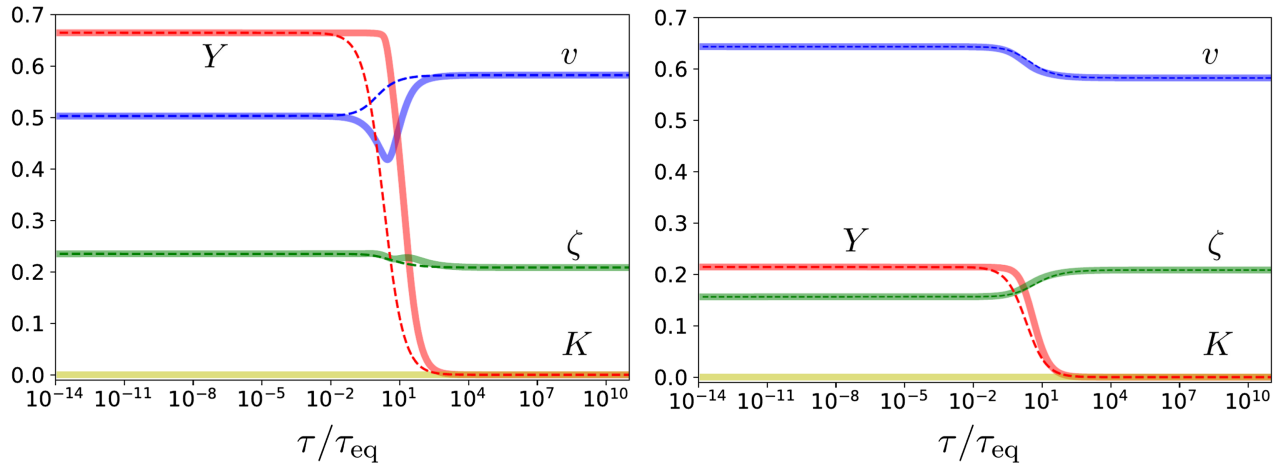

FIG. 1. Evolution of the CVOS variables using the full system (3) (thick solid transparent lines) and the one-parameter approximation (12) (dashed lines). The exact case is solved using the α–dependent leakage function $A(Y)$ given by (6), which allows the value for $Y_{\rm SC}$ to be set in (10) as required for solving (12). Two different time evolutions are shown with different mass ratio parameters, namely $\alpha = 1$ (left panel) and $\alpha = 3$ (right panel). Note that in both cases, differences are only visible around the radiation-matter transition, whose influence in the cosmological consequences is negligible, thereby justifying the one-parameter approximation.

The actual value of $Y_{\rm SC}$ depends on the type of cosmic string under consideration (in particular, it should be a function of the parameter α) and the available physical mechanisms for the current leakage. It follows that we can simplify the system (3) by assuming that the charge Y evolves phenomenologically as

$$Y_{\rm f} = Y_{\rm SC}\left(2 - \frac{\dot{a}}{a}\tau\right) = \frac{2Y_{\rm SC}\tau_{\rm eq}}{\tau + 2\tau_{\rm eq}}, \tag{10}$$

where the exact solution [57]

$$a(\tau) = a_{\rm eq}\left[2\left(\frac{\tau}{\tau_{\rm eq}}\right) + \left(\frac{\tau}{\tau_{\rm eq}}\right)^2\right], \tag{11}$$

connecting the radiation and matter dominated eras, was used.

By changing $Y_{\rm SC}$, we obtain generic predictions that allow us to distinguish current-carrying from ordinary cosmic strings. Thus, in what follows we treat $Y_{\rm SC}$ as a free parameter that spans all possible scenarios of CMB anisotropies generated by a chiral current-carrying cosmic string network. In that case the CVOS together with (10) can be written as

$$\begin{cases} \frac{{\rm d}\xi_{\rm c}}{{\rm d}\tau} = \frac{\xi_{\rm c}v^2}{1+Y_{\rm f}}\frac{\dot{a}}{a} + \frac{cv}{2} + \frac{Y_{\rm f}}{1+Y_{\rm f}}vk(v), \\ \frac{{\rm d}v}{{\rm d}\tau} = \frac{(1-v^2)}{1+Y_{\rm f}}\left[\frac{k(v)(1-Y_{\rm f})}{\xi_{\rm c}} - 2v\frac{\dot{a}}{a}\right]. \end{cases} \tag{12}$$

Solving the above system using the value of $Y_{\rm SC}$ provided by the solution of the full system (3) allows us to assess the validity of the approximation. Such a comparison is shown as an illustration in Fig. 1.

To compare the one-parameter model with the complete evolution depicted in Fig. 1, we can use Eq. (10). However, when dealing with CMBACT, it becomes necessary to incorporate a Heaviside function, denoted as $\Theta(\ldots)$, to prevent the charge value from reaching negative values:

$$Y_{\rm f} = Y_{\rm SC}\left(2 - \frac{\dot{a}}{a}\tau\right)\Theta\left(2 - \frac{\dot{a}}{a}\tau\right). \tag{13}$$

Despite the small deviation of the Y function close to the radiation-matter transition period, the simple model described by Eqs. (12) reproduces the CVOS time development quite well throughout most of the evolution of the universe. Using this simplified model, we are able to scan the relevant parameter space by varying the value of a single parameter, $Y_{\rm SC}$ (cf. Sec. III A below). Using a modified version of CMBACT [51] applied to the CVOS model, as briefly described in Appendix, we can obtain the cosmological consequences expected from a current-carrying cosmic string network in the CMB.

A. The single-parameter model

As previously explained, we focus our analysis on the model with a single parameter $Y_{\rm SC}$ described by the simplified system (12) with (13). It is then sufficient to vary the parameter $Y_{\rm SC}$ and calculate how it impacts the CMB anisotropy predictions. Substituting the dynamics of the system under consideration described by Eqs. (12) as functions of the redshift rather than time, shown in Fig. 2, the stress-energy tensor components required for the CMBACT code [51] are found from the expressions (A6) for the different values of $Y_{\rm SC}$. The scalar-vector-tensor decomposition contributions from the string network are

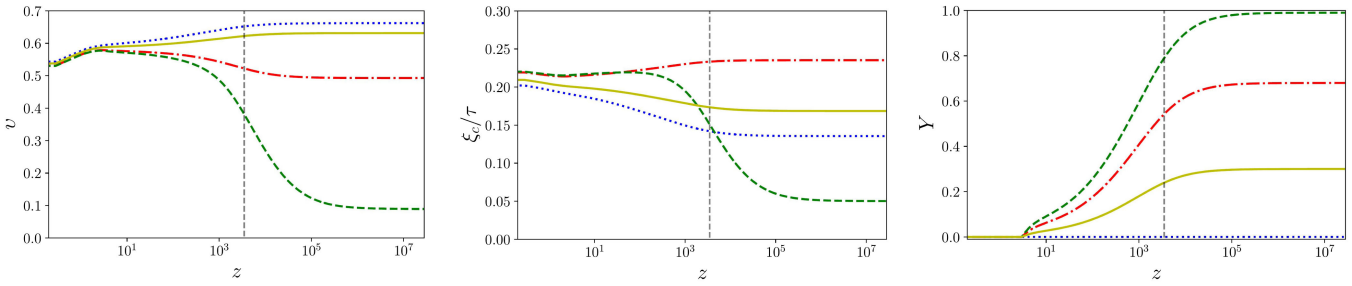

FIG. 2. Evolution of current-carrying cosmic strings thermodynamical quantities $v(z)$ (left panel), $\epsilon(z)$ (middle) and $Y(z)$ (right) as functions of the redshift z for three different values of the scaling radiation charge, namely $Y_{\rm sc} = 0.99$ (green dashed), $Y_{\rm sc} = 0.68$ (red dot-dashed) and $Y_{\rm sc} = 0.3$ (yellow solid). These are compared with the uncharged Nambu-Goto evolution (blue dotted). Note that contrary to Fig. 1 which was calculated using the radiation and matter solution (11), this figure, as the CMBACT calculations below, is drawn using the full solution including the present cosmological constant dominated era. This explains in particular the sudden drop in the total charge for redshifts of a few.

shown in Fig. 14 in Appendix, while the resulting late-time matter power spectrum $P(k)$ is shown in Fig. 3. The angular power spectrum of CMB anisotropies are shown in Fig. 4, which depicts the temperature (T) and E– and B–polarization correlations C_{TT}, C_{TE}, C_{EE} and C_{BB}.

The CMB and dark matter perturbation spectra result from the interplay of scalar, vector and tensor contributions from strings moving at relativistic velocities, which are more complex than inflationary fluctuations dominated by adiabatic scalar modes. The subtle effect of altering the magnitude of string currents is illustrated in the matter power spectrum $P(k)$ shown in Fig. 3. A small scaling charge makes hardly any difference compared with the NG case, as expected, but when the charge increases and there is significant reduction in the string velocity, then there is less power on all scales, although predominantly at small ones. At this point, the primary perturbative effect of strings

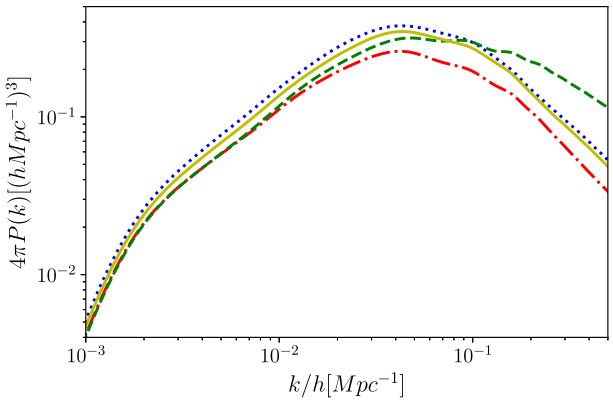

FIG. 3. Power spectra predicted for current-carrying cosmic strings with the same values and conventions as in Fig. 2. The predicted power spectrum is not a simple function of the scaling radiation charge $Y_{\rm SC}$, the intermediate value $Y_{\rm sc} = 0.68$ (red dot-dashed line) leading to less power than the lowest one $Y_{\rm sc} = 0.3$ (yellow solid). On small scales, the power is significantly larger for the highest value $Y_{\rm sc} = 0.99$ (green dashed line).

remains through their motion, creating "wakes" in the dark matter distribution or discontinuities in the CMB temperature [58,59].

Increasing the scaling charge to $Y_{\rm SC} = 0.99$ causes the velocity to drop even further with the network density rising higher due to the smaller spacing between cosmic strings at these larger charges. In this case, the charged string power spectrum in Fig. 3 begins to exceed the NG prediction on small scales. This effect is also reinforced by the reduced string velocity because there is a cross-over between the gravitational effects of the string motion and the scalar Newtonian potential generated by the charge along the string (absent for a straight NG string). In general, the maximal amplitude of the power spectrum decreases for current-carrying cosmic strings and moves toward smaller length scales. This phenomenon could conceivably hold intriguing implications for early structure formation, as proposed in Ref. [60], establishing some of the necessary conditions for the formation of massive black holes at high redshifts originating from current-carrying strings, as discussed in Ref. [61].

The various CMB correlation functions are shown in Fig. 4, and they demonstrate a similar nontrivial effect with the increase of the scaling charge $Y_{\rm SC}$. The temperature autocorrelation starts decreasing with the charge, with an overall amplitude drop a factor which we found to be at most of the order 25%; this could presumably lead to a slight easing of the cosmic strings constraint from current CMB observations. On the other hand, for larger charges there is a cross-over which leads to larger temperature anisotropies on smaller scales, as noted already for the matter power spectrum. The relative contributions of the scalar, vector, and tensor modes to the temperature auto-correlations are shown in Fig. 5.

The TE cross correlation is hardly affected at all by the presence of a current flowing along the long strings, expect for very high charges. The same conclusion holds for the EE polarization, though an enhancement of

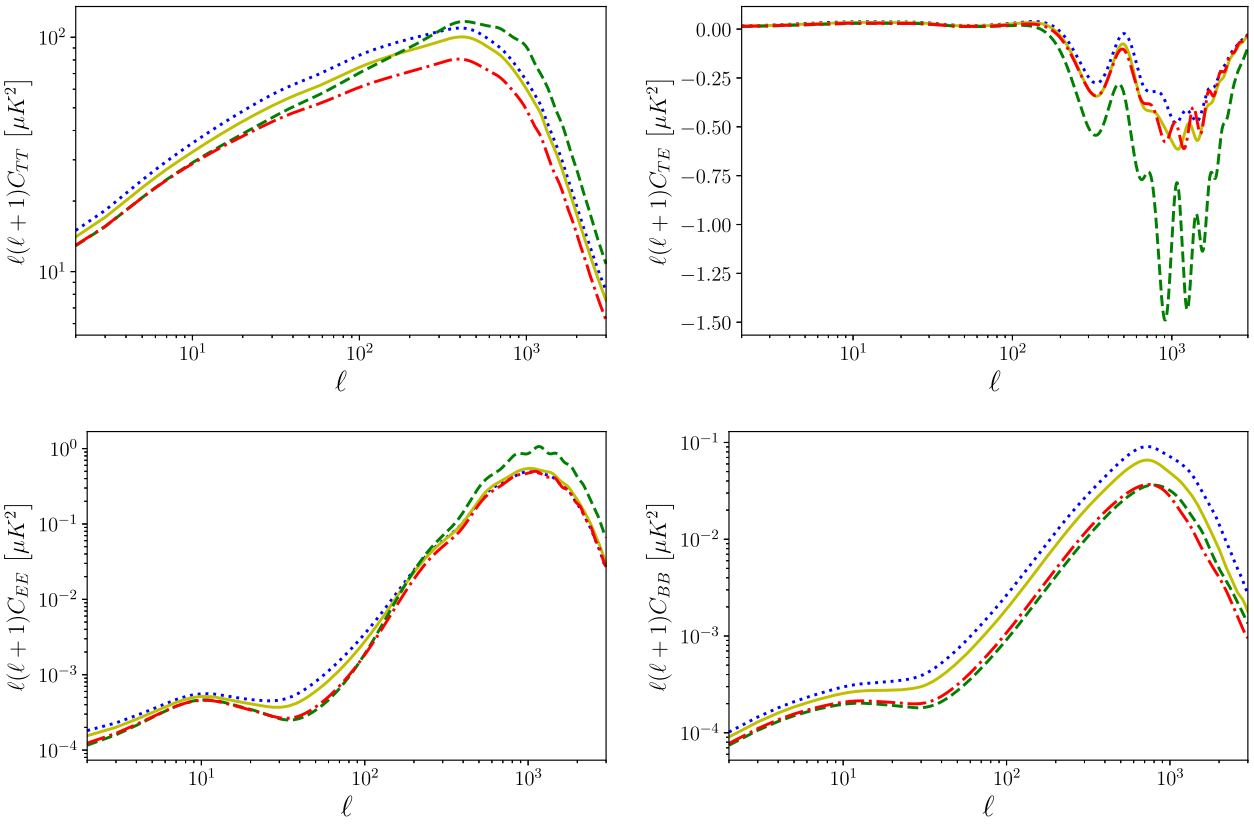

FIG. 4. CMB anisotropies predicted for a current-carrying cosmic string network in the different observable modes, namely C_{TT} (upper left panel), C_{TE} (upper right), C_{EE} (lower left) and C_{BB} (lower right), up to the normalization factors $\ell(\ell+1)$, as functions of the multipole ℓ. These curves are shown for the same values and conventions as those in Fig. 2 and represent the sum over all the contributions (scalar, vector and tensor)—details are presented in Appendix. Although the largest effect comes from the largest scaling charge for the TT, TE and EE modes, the BB mode contribution is larger for the Nambu-Goto case.

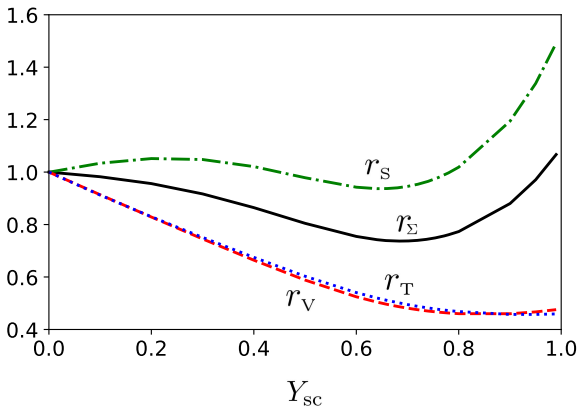

FIG. 5. The ratios $r_{\rm I} = \max\,[C^{\rm I}_{TT}(Y_{\rm SC})/C_{TT}(0)]$, with $\rm I = S$ (scalar contribution), $\rm I = V$ (vectors), and $\rm I = T$ (tensors) between the maxima of the relevant modes for the current-carrying case and the corresponding values for a Nambu-Goto network. The sum over all modes is shown as $\rm I = \Sigma$. At most, one finds that the total amplitude can be reduced by a factor of around 25% so that inclusion of current-carrying capabilities in a cosmic string network cannot substantially modify the existing constraints on the string energy scale.

roughly a factor of two can be observed at high charge. Finally, the distinctive string network BB correlation appears to be a roughly monotonically decreasing function of the scaling charge, halting at a plateau above which its maximum amplitude is half of the NG prediction. The BB contribution from vector and tensor modes is due to the string velocity which is suppressed by the presence of large charges.

B. Other relevant scenarios

On top of the above models, described mainly by a single parameter, Ref. [31] (and Fig. 1 therein) identified 4 particular models, unimaginatively called (a), (b), (c) and (d), whose redshift evolution is displayed in Figs. 6 and 7. These models represent different scenarios of current-carrying string network evolution, and the aforementioned work discusses how they span the possible range of physically realistic evolution scenarios. Let us now give a brief description for each case.

The models described above assume no bias in the loop chopping efficiency, with respect to charge and current, but

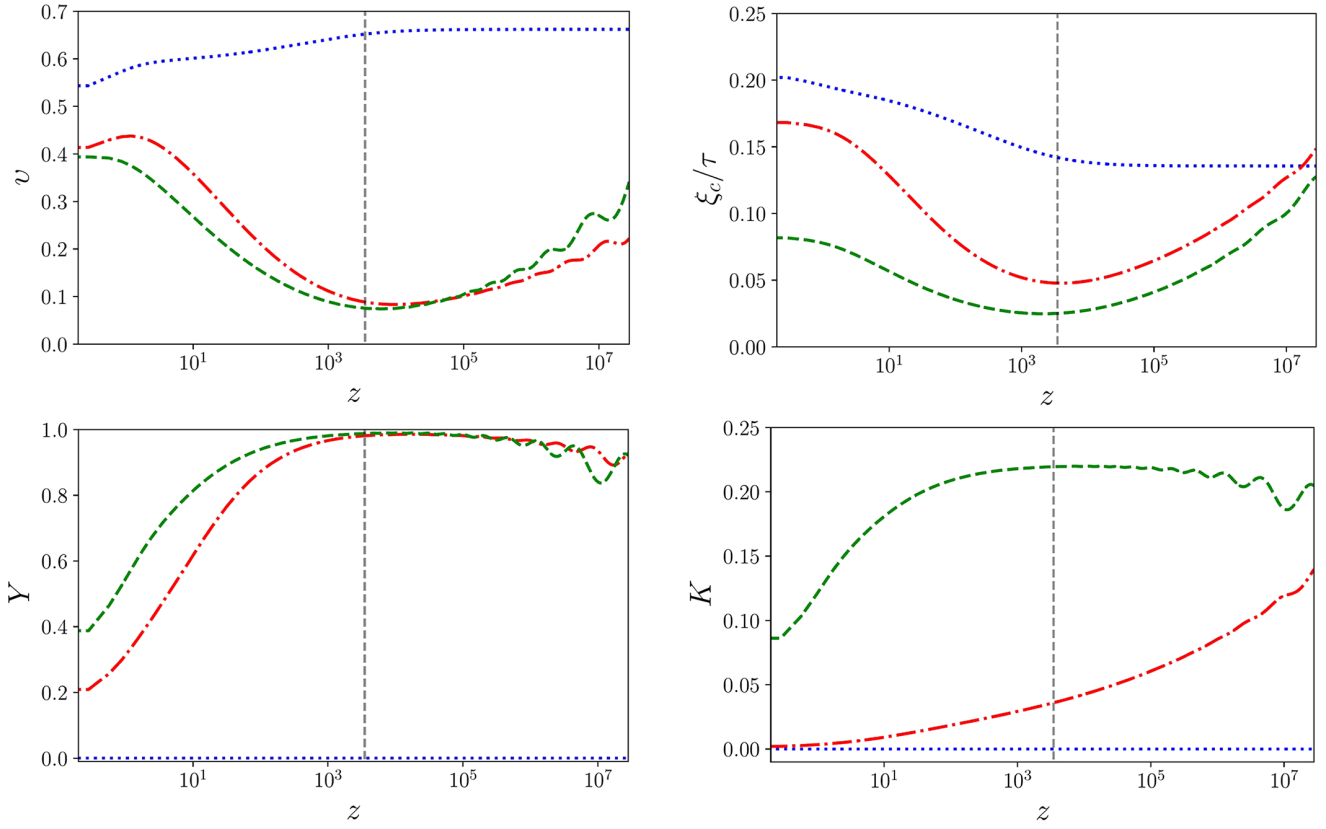

FIG. 6. Evolution of the thermodynamical quantities $v(z)$, $\epsilon(z)$ and $Y(z)$ as function of the redshift z for the models denoted (a) (dot-dashed red line) and (c) (dashed green) in Ref. [31] as well as the standard Nambu-Goto evolution (dotted blue) for comparison. Both models have vanishing leakage $A_c = 0$, constant momentum parameter $k_{(a)} = 0.6$ and $k_{(c)} = 0.4$, and bias $g_{(a)} = 0.9$ and $g_{(c)} = 1$, model (a) having a slightly higher than Nambu-Goto chopping efficiency $c_{(a)} = 0.5$. The absence of leakage lead to so-called frozen configurations in which the RMS velocity v and correlation length decrease in the radiation era. In both cases, the charge Y saturates during the radiation era. The chirality takes a nonvanishing scaling value in the radiation era for model (c) but it falls monotonically for model (a). Both models also have a nonvanishing charge throughout the matter era, albeit decreasing.

this can also be included. Specifically, when a NG long string network loses energy through loop formation, the chopping efficiency c is defined by [33]

$$\left.\frac{\mathrm{d}E_{\mathrm{NG}}}{\mathrm{d}\tau}\right|_{\mathrm{loops}} = -cv\frac{E_{\mathrm{NG}}}{\xi_{\mathrm{C}}}, \tag{14}$$

while for a current-carrying network, this relation becomes [31]

$$\left.\frac{\mathrm{d}E}{\mathrm{d}\tau}\right|_{\mathrm{loops}} = -g(Y,K)cv\frac{E}{\xi_{\mathrm{C}}}, \tag{15}$$

thereby introducing the bias function g which *a priori* depends on both the charge Y and the chirality K. The single-parameter model of the previous section shares with the NG scenario the unbiased property, in that it assumes $g = 1$, contrary to the particular cases which we now discuss.

More details about these four models can be found in Ref. [31]. The redshift developments of the frozen category of models (a) and (c), with behavior (16), are shown in Fig. 6, while the more regular (b) and (d) scenarios with linear scaling behavior (8) are shown in Fig. 7. For convenience, we show the evolution of the rms velocity v, charge amplitude Y and conformal characteristic length $\xi_{\mathrm{C}}^2 = \mu_0(1+Y)/(\rho a^2)$ (with ρ the string network density) for frozen networks in Fig. 6. In particular, we see that during the radiation period there is a power law decay of v and ξ_{C}/τ according to Eq. (16), while the charge amplitude Y tends to its saturated value $Y_{\mathrm{sat}} = 1$ as a power law as well. One can see that the choice of parameters in the model "(c)" leads to much smaller values of ξ_{C}/τ in comparison with the model "(a)".

1. Model (a): Frozen chiral

The first particular case of interest we studied in Ref. [31] corresponds to what we called a frozen string

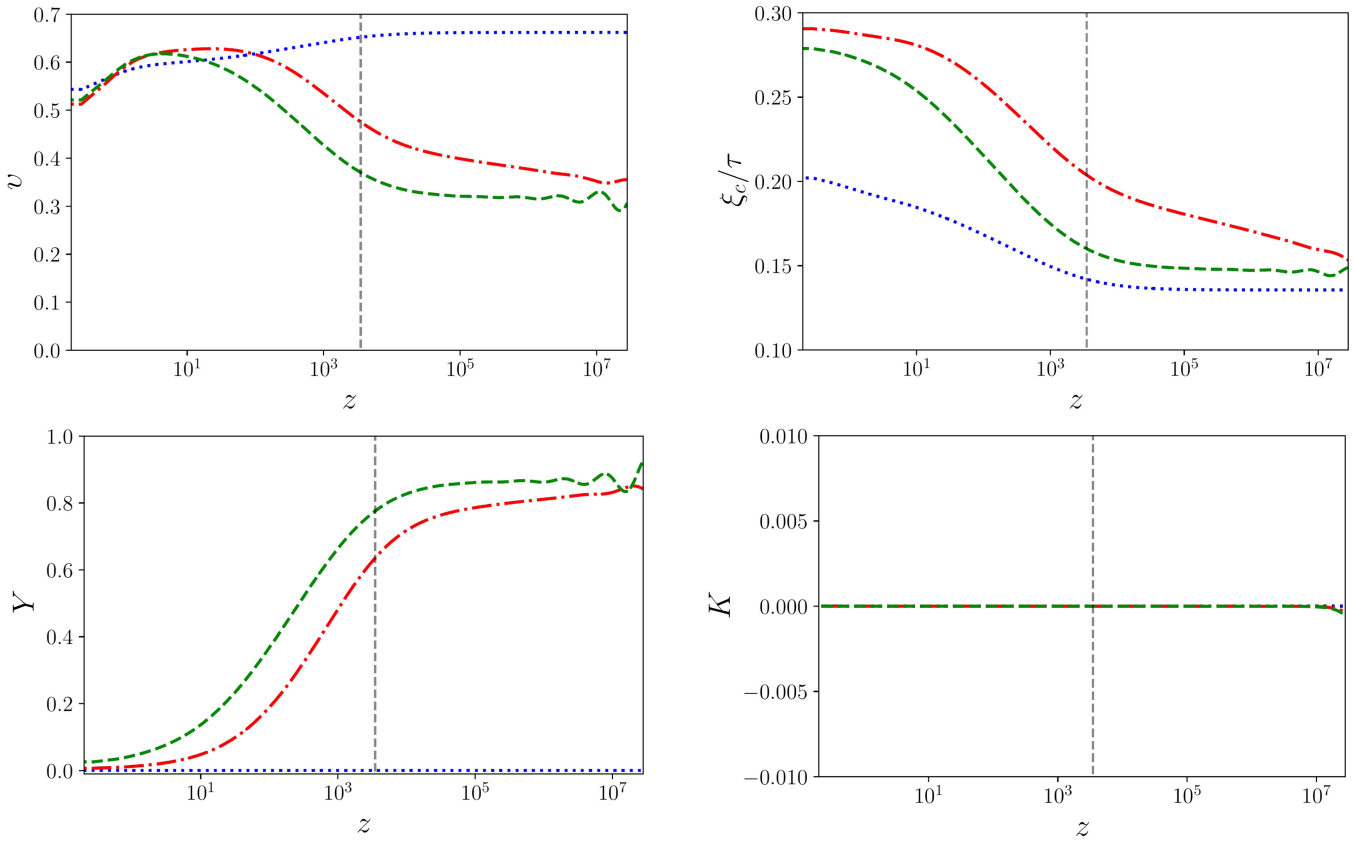

FIG. 7. Evolution of the thermodynamical quantities $v(z)$, $\epsilon(z)$ and $Y(z)$ as functions of the redshift z for the models denoted (b) (dot-dashed red line) and (d) (dashed green) in Ref. [31] as well as the standard Nambu-Goto evolution (dotted blue) for comparison. Model (b) has no leakage ($A_c = 0$) and a bias function (see text) $g = 1 + 1.2Y$, while model (d) has no bias and a large constant leakage $A(Y) = 0.6$. Both models assume a constant momentum parameter $k = 0.7$ and can be seen to belong to the radiation scaling cases.

network. Assuming no (or negligible) losses, i.e. setting $A_c = 0$ in Eq. (6), the charge tends to saturate to the constant value $Y_{SC} \to 1$ while the velocity decreases to vanishingly small values, hence the "frozen" network qualification. In this model, the momentum parameter is given a constant value, in practice we chose $k(v) = k_{(a)} = 0.6$, which is compatible with the fact that as the velocity decreases, $k(v)$ varies very little and eventually reaches a plateau for $v \ll 1$. We also set the chopping efficiency c to the value $c_{(a)} = 0.5 > c_{NG}$, slightly larger than the value obtained in NG simulations, and assumed a constant bias $g(Y, K) = g_{(a)} = 0.9$: the value of the bias parameter g controls whether loops typically lose above ($g > 1$) or below ($g < 1$) the average current and charge from the network.

These assumptions lead to nontrivial current during the whole string network evolution, and indeed, we find that even during the matter dominated era, the charge gets a nonvanishing value. In the absence of any relevant charge leakage mechanism in this scenario, the string network is frozen during the radiation period, and we found that the thermodynamical quantities evolve according to [31]

$$v \propto \frac{\xi_C}{\tau} \propto \sqrt{1 - Y} \propto \tau^{-s}, \tag{16}$$

where s is a positive constant: during the radiation-dominated era, the long string network stops moving and it becomes denser, with the correlation length decreasing. The matter dominated epoch is characterized by the approach to scaling of the network, as defined in Eq. (8), including a nontrivial charge $Y \neq 0$ value.

This scenario is also denoted "chiral" because although the charge Y saturates to unity, this number being a consequence of our choice of the linear equation of state (it can be above or below in the nonlinear regime [32]), the chirality K rapidly decreases even if given an initial nonvanishing value.

2. Model (b): Linear scaling

This type of model shows a nontrivial scaling charge $Y \neq 0$ in the radiation epoch, i.e. the full scaling behavior of Eq. (8), followed by an ordinary Nambu-Goto string network with vanishing charge $Y = 0$ in the matter dominated epoch. In this case, looking rather similar to the

one-parameter model of Sec. III A, the bias parameter g of Eq. (15) is made into a function of the charge (we restrict attention to a linear behavior as a first guess), namely

$$g = 1 + bY, \tag{17}$$

and we set a positive value for the constant b. As in the previous case, we consider a negligible leakage $A_c = 0$ but a larger momentum parameter $k_{(b)} = 0.7$.

3. Model (c): Frozen nonchiral

Changing only slightly the parameters of model (a) yields a different situation in which although the charge saturates to $Y \to 1$ in the radiation dominated era, there is a nonvanishing chirality (positive in this case). Here, the chopping efficiency is set to its NG value $c_{NG} = 0.23$, while the momentum parameter is still assumed constant, but smaller, namely $k_{(c)} = 0.4$, and there is no bias, i.e. $g_{(c)} = 1$. In this case, the nonchiral and charged radiation dominated era is followed by the approach to matter-dominated scaling in which both the charge and the chirality decay to negligible values (i.e. asymptotically the NG network scaling solution without charge or current).

4. Model (d): Linear scaling with leakage

The final special case is also rather close to the previous single-parameter case, also exhibiting the standard scaling behavior of Eq. (8) with nontrivial charge $Y \neq 0$ during the radiation dominated epoch which vanishes after the radiation to matter domination transition. The parameters are chosen such that the momentum parameter is set $k_{(d)} = 0.7$ [larger than in (a) and (c)], the chopping efficiency as for the NG case, and with no bias, but the key difference is that we assume a constant leakage function $A(Y) = A_{(d)} = 0.6$.

IV. CMB PREDICTIONS

By using the Eqs. (A6) in the Appendix together with the evolution of CVOS models which for the four CVOS model examples of Ref. [31] in the CMBACT code, we can now obtain the corresponding CMB anisotropy predictions. The first conclusions that can be drawn concern the matter power spectrum shown in Fig. 8 for the cases (a) and (c) and in Fig. 9 for (b) and (d). Not unexpectedly, the power spectrum from the models (b) and (d), whose behavior is quite similar to that of the single-parameter approximation, also predicts relatively small deviations from the NG spectrum, with potentially less power on large scales and more on small scales, as shown in Fig. 9. The frozen cases (a) and (c), on the other hand, show much more noticeable deviations from the standard behavior, with an amplified spectrum across all scales, though most notably at small length scales, where the discrepancy can reach the level of one or two orders of magnitude. If such models are physically realistic, then very stringent constraints on the underlying parameters will ensue.

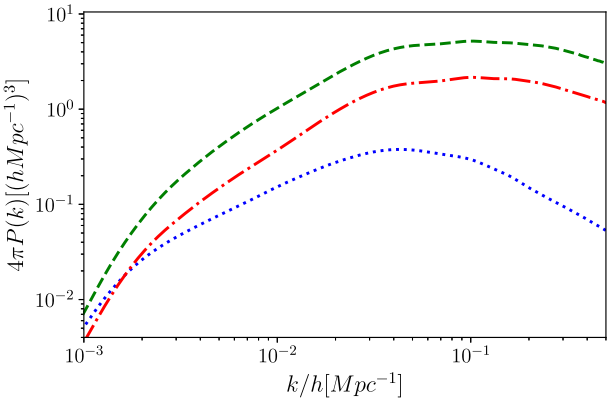

FIG. 8. Power spectra for current-carrying cosmic strings described by the so-called frozen models (a) and (c). The parameter choices and color conventions follow the same notation as in Fig. 6.

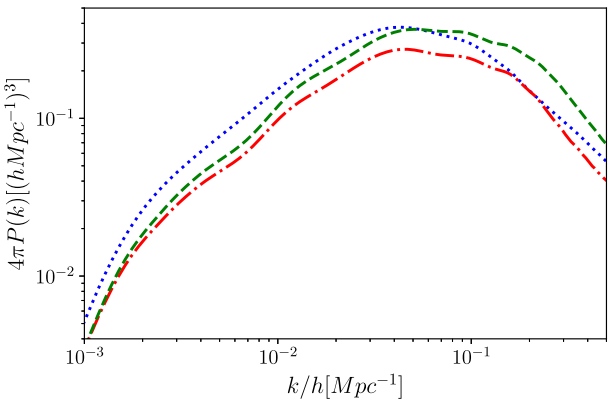

FIG. 9. Power spectra for current-carrying cosmic strings described by (b) and (d) models. The parameter choices and color conventions follow the same notation as in Fig. 7.

The resulting CMB anistropies for models (a) and (c) are illustrated in Fig. 10. The larger scalar modes from model (c) yield larger TT and EE auto-correlations. The minimum velocities for (a) and (c) examples are close to each other, as are the $1 - Y$ values which results in a similar magnitude for the vector and tensor modes, which are significantly reduced compared to the Nambu-Goto case, as seen in the Appendix Fig. 15. On the other hand, the more dense model (c) leads to a larger vector mode contribution than the model (a). Still, both contributions, from the (a) and (c) models, reduce vector modes significantly in comparison to the standard Nambu-Goto cosmic strings. The increase of the contribution of current-carrying cosmic strings can be observed only for high multipole moments $\ell > 10^3$ of the vector modes.

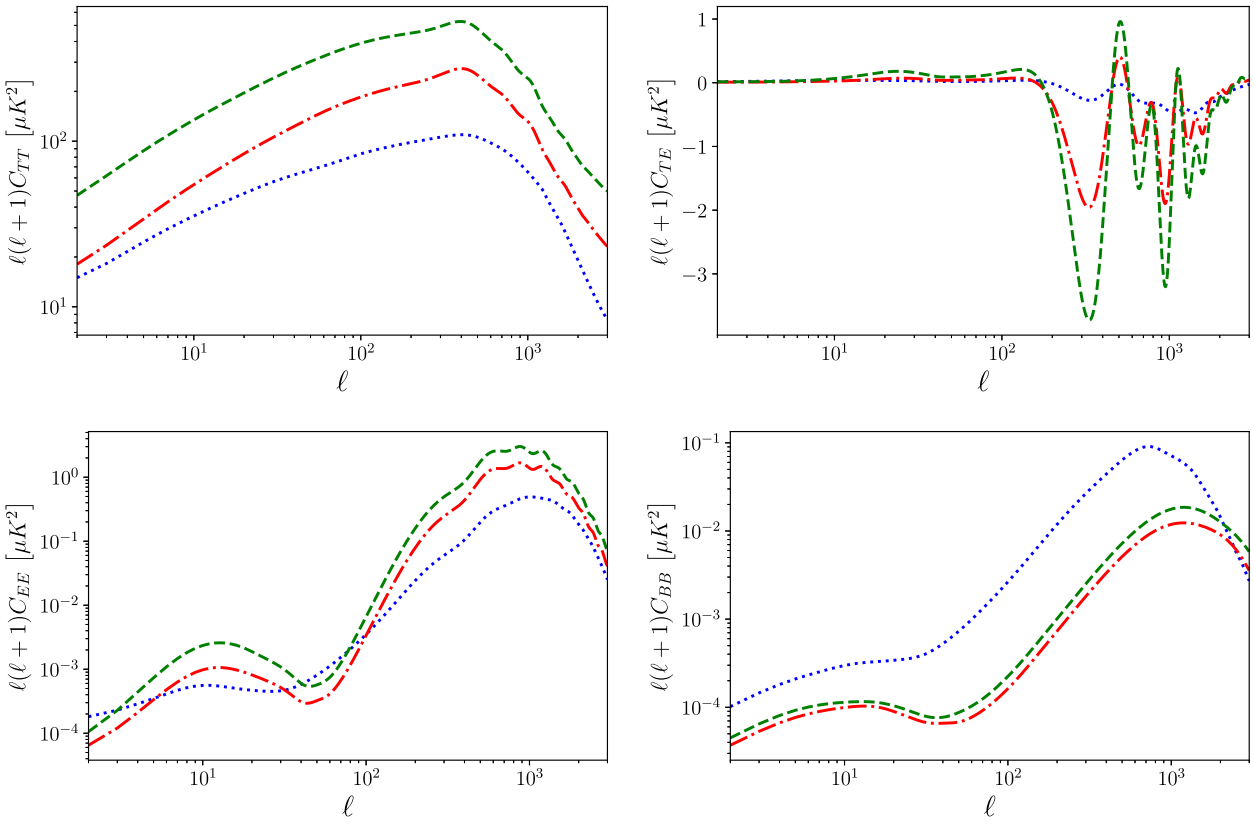

FIG. 10. CMB anisotropies predicted for a from current-carrying cosmic string network in the different observable modes, namely C_{TT} (upper left panel), C_{TE} (upper right), C_{EE} (lower left) and C_{BB} (lower right), up to the normalization factors $\ell(\ell+1)/(2\pi)$, as functions of the multipole ℓ. These curves are shown for the same value and color convention as those in Fig. 6 and represent the sum over all the contributions (scalar, vector and tensor). Further details are presented in Appendix. Dot-dashed red lines represent model (a), dashed green lines—model (c) as defined in Ref. [31] and dotted blue lines—Nambu-Goto.

The particular increase of vector modes for high multipole moments ℓ occurs only for string networks that go through a frozen type of evolution. The frozen network clearly changes the relation $\ell(1+\ell)C_{TT} \propto \ell^{-1.5}$ [62,63] for long strings. Carrying out the fit for $\ell > 2500$, as illustrated in Fig. 11, we obtain that the models (a) and (c) behave as

$$\ell(1+\ell)C_{TT}^{(\mathrm{a})} \propto \ell^{-0.67}, \qquad \ell(1+\ell)C_{TT}^{(\mathrm{c})} \propto \ell^{-0.50}, \tag{18}$$

providing a potential signal for small-scale anisotropy [63]. However, one should keep in mind, that the presence of loops will eventually dominate for $\ell \gtrsim 2000$, assuming the relation $\ell(1+\ell)C_{TT}^{\mathrm{loops}} \propto \mathrm{const.}$ obtained in Ref. [37].

The CMB anisotropies for models exhibiting linear scaling regimes (b) and (d) are depicted in Fig. 12. As anticipated, these models demonstrate behavior akin to the single-parameter approximation. This similarity is visually

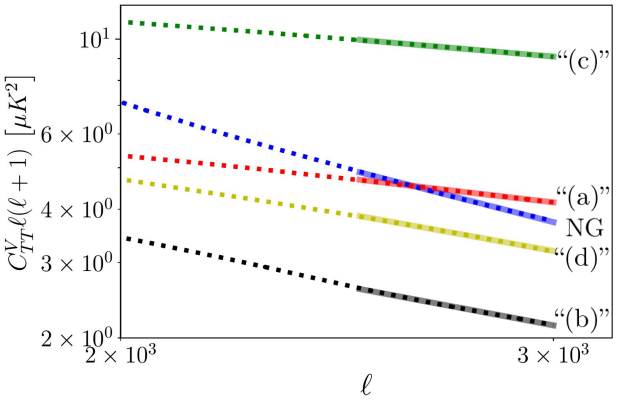

FIG. 11. Fit of vector modes (represented by straight lines) as the dominant $\ell > 800$ component for CMB anisotropies $C_{TT}^{V}(\ell)$ (represented by dots) produced by current-carrying cosmic string networks described by models (a) to (d) models, as well as the Nambu-Goto case (NG). The best-fit exponents (18) for models (a) to (d) are as follows: -0.67, -1.1, -0.5, and -1, with -1.5 for NG.

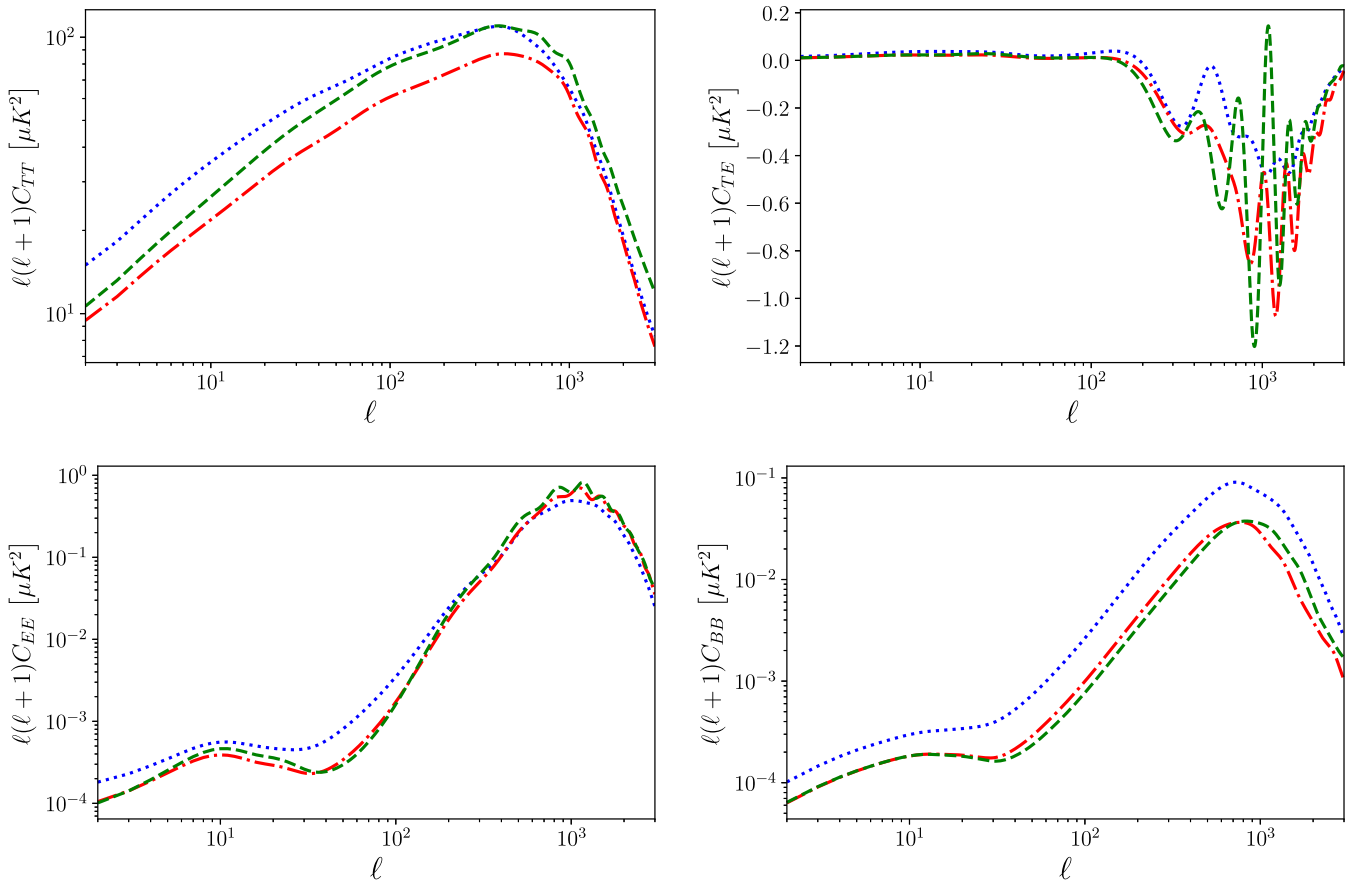

FIG. 12. CMB anisotropies predicted for a from current-carrying cosmic string network in the different observable modes, namely C_{TT} (upper left panel), C_{TE} (upper right), C_{EE} (lower left) and C_{BB} (lower right), up to the normalization factors $\ell(\ell+1)$, as functions of the multipole ℓ. These curves are shown for the same value and convention as those in Fig. 7 and represent the sum over all the contributions (scalar, vector and tensor)—details are presented in Appendix. Dot-dashed red lines represent model (b), dashed green lines—model (d) as defined in Ref. [31] and dotted blue lines—Nambu-Goto.

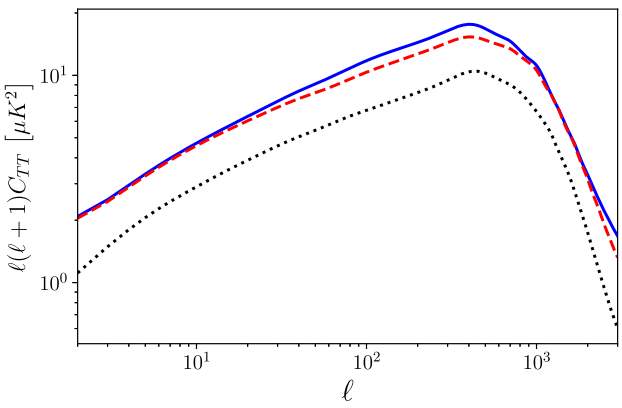

FIG. 13. Comparison between the C_{TT} modes of the full model (solid blue line), described by Eqs. (3), and the single-parameter approximation (dashed red line), given by Eqs. (13) and (12). In the single-parameter model, we set $Y_{\rm sc} = 0.9$, whereas in the full model, we adjusted parameters to ensure that during the radiation period, the scaling value of the charge amplitude $Y_{\rm rd} = 0.9$. Additionally, for comparison purposes, we present the standard Nambu-Goto result with a black dotted line.

evident when comparing Fig. 4 with Fig. 12, indicating that the single-parameter approximation effectively captures the main features of the (b) and (d) models. This is also evidenced by direct comparisons between the CMB anisotropies obtained from this simplification and those from the full parameter model, as shown in Fig. 13. The small differences observed, which do not exceed 15% even for large current values $Y \sim 0.9$, suggest that the single-parameter approximation offers useful insights for the CMB anisotropies generated by current-carrying cosmic string networks, at least for those models exhibiting a linear scaling regime of evolution.

V. CONCLUSIONS

We have provided a first study of the CMB anisotropy for current-carrying strings, relying on our previously developed CVOS model. We have shown that as the charge is increased, there is a minimum contribution to the TT correlation. In particular, one can see the sum of TT components in Fig. 4. The dashed line in this plot, with

$Y_{\rm SC} = 0.68$, is approximately the smallest contribution that can be obtained for the TT correlation due to the presence of the current, according to the CVOS model with equation of state (1). This minimal value can be also seen in Fig. 5, where $r_\Sigma = \max[C_{TT}(Y_{\rm SC})/C_{TT}(0)]$ has a minimum at $Y_{\rm SC} \approx 0.68$ with an amplitude reduction of around 25%.

In Fig. 5 we also see that the maxima for the vectors $r_{\rm v} = \max[C^{\rm v}_{TT}(Y_{\rm SC})/C_{TT}(0)]$ and tensors $r_{\rm T} = \max[C^{\rm T}_{TT}(Y_{\rm SC})/C_{TT}(0)]$ decreases monotonically as the current contribution increases. Hence, the increase of the ratio of scalar to vector/tensor modes plays a characteristic role in the CMB anisotropy signal that can distinguish standard Nambu-Goto strings from cosmic strings with nontrivial internal structure.

As a final caveat, we note that our results are based on two levels of approximation. The first stems from the simplifying assumptions of piecewise source terms in the CMBACT Einstein-Boltzmann code. The second pertains to the CVOS network evolution model itself. Although this builds upon the standard VOS model, which has been the subject of extensive testing and calibration (including both field theory and Nambu-Goto simulations), the analogous process of calibration has not yet been achieved for the CVOS extension per se. The reason for this is simply the absence of reliable simulations of the evolution of string networks with charges and currents. It is our understanding that such simulations are now becoming available, so a more detailed and robust study of the cosmological consequences of these networks will become possible in the near future.

It is essential to note that our analysis does not include certain potentially intriguing phenomena that could have an influence on the evolution of a current-carrying string network. Specifically, we have not incorporated the effect of primordial magnetic fields that may arise from an early universe phase transition as, for example, discussed in Ref. [64]. In principle, such a magnetic field could generate currents along the strings, nontrivially modifying the evolution of cosmic string networks (see, e.g., Ref. [65]). This fascinating avenue remains open for further exploration.

ACKNOWLEDGMENTS

This work was financed by Portuguese funds through FCT—Fundącão para a Ciência e a Tecnologia in the framework of the project 2022.04048.PTDC (Phi in the Sky, DOI 10.54499/2022.04048.PTDC) and R&D project 2022.03495.PTDC (uncovering the nature of cosmic strings). C. J. M. also acknowledges FCT and POCH/FSE (EC) support through Investigador FCT Contract 2021.01214.CEECIND/CP1658/CT0001 (DOI 10.54499/2021.01214.CEECIND/CP1658/CT0001). P. S. acknowledges funding from the STFC Consolidated Grants No. ST/P000673/1 and No. ST/T00049X/1. I. R. also acknowledges support from the Grant No. PGC2022-126078NB-C21 funded by MCIN/AEI/10.13039/501100011033 and "ERDF A way of making Europe", as well as Grant DGA-FSE Grant No. 2020-E21-17R from the Aragon Government and the European Union—NextGenerationEU Recovery and Resilience Program on 'Astrofísica y Física de Altas Energías' CEFCA-CAPA-ITAINNOVA.

APPENDIX: CMBACT FOR CVOS

We use a modified version of the publicly available CMBACT code [51] to describe the CMB anisotropies generated by current-carrying cosmic strings, in comparison with standard NG scenario. Our primary goal is to identify differences that may lead to future discriminating tests between the two types of strings.

Here we provide a concise description of the methodology employed in the CMBACT code [51,66] for calculating anisotropies generated by cosmic strings, including the extension for current-carrying strings. The CMBACT code is built upon the CMBFAST linear Einstein-Boltzmann equations solver, which requires the stress-energy tensor of the active source as an input. Consequently, it is essential to obtain a Fourier-transformed stress-energy tensor that accurately represents the string network.

The CMBACT code utilizes randomly oriented straight segments to approximate a realistic string network. These straight segments have a length ξ and move in random directions with a velocity v, gradually decaying while ensuring that their total energy corresponds to that of the VOS (or CVOS) model. Therefore, we can represent the collection of straight segments as follows [51]:

$$X^\mu = x^\mu_0 + \sigma \hat{X}^\mu_1 + \tau \hat{X}^\mu_2, \tag{A1}$$

where

$$\hat{X}^\mu_1 = \begin{pmatrix} 0 \\ \sin\theta\cos\phi \\ \sin\theta\sin\phi \\ \cos\theta \end{pmatrix} \tag{A2}$$

and

$$\hat{X}^\mu_2 = \begin{bmatrix} 1 \\ v(\cos\theta\cos\phi\cos\psi - \sin\phi\sin\psi) \\ v(\cos\theta\sin\phi\cos\psi + \cos\phi\sin\psi) \\ -v\sin\theta\cos\psi \end{bmatrix}, \tag{A3}$$

and v is the rms velocity. Three angles, θ, ϕ and ψ correspond to the random selection of the string's orientation,

whereas σ and τ parameterise the string world sheet of straight segments.

We employ the macroscopic variables from the CVOS model, rather than the VOS model, to describe straight string segments in Eq. (A1). As a result, the stress-energy tensor for the current-carrying string network can be expressed as the sum of the stress-energy tensors of all individual straight segments. The stress-energy tensor for each straight segment of a current-carrying string can be written using the macroscopic CVOS variables in the following way [67]

$$T^{\mu\nu} = \frac{\mu_0}{\sqrt{-g}} \int \mathrm{d}^2\sigma \sqrt{-\gamma}\,\delta^{(4)}(x^\lambda - X^\lambda) \times \left[\tilde{U}\tilde{u}^\mu\tilde{u}^\nu - \tilde{T}\tilde{v}^\mu\tilde{v}^\nu - \Phi(\tilde{u}^\mu\tilde{v}^\nu + \tilde{v}^\mu\tilde{u}^\nu)\right], \tag{A4}$$

where we have defined $\tilde{U} \equiv 1 + Y$, $\tilde{T} \equiv 1 - Y$, $\Phi \equiv \sqrt{Y^2 - \frac{1}{4}K^2}$, $\tilde{u}^\mu \equiv \dot{X}^\mu/\sqrt{\dot{X}^2}$, and $\tilde{v}^\mu \equiv X'^\mu/\sqrt{-X'^2}$. The Fourier-transformed stress-energy tensor is given by

$$\Theta^{\mu\nu} = \mu_0 \int_{-\xi_c/2}^{\xi_c/2} \left[\tilde{U}\frac{\dot{X}^\mu\dot{X}^\nu}{\sqrt{1-v^2}} - \tilde{T}\sqrt{1-v^2}\,X'^\mu X'^\nu - \Phi(\dot{X}^\mu X'^\nu + X'^\mu\dot{X}^\nu)\right] \mathrm{e}^{i\boldsymbol{k}\cdot\boldsymbol{X}}\mathrm{d}\sigma, \tag{A5}$$

where, without loss of generality, we use the wave vector oriented along the third component: $\boldsymbol{k} = k\boldsymbol{e}_3$. Carrying out the integration in Eq. (A5) one can obtain expressions for the scalar $\Theta^{\mathrm{S}} \equiv \frac{1}{2}(2\Theta_{33} - \Theta_{11} - \Theta_{22})$, vector $\Theta^{\mathrm{V}} \equiv \Theta_{13}$ and tensor $\Theta^{\mathrm{T}} \equiv \Theta_{12}$ parts (see Sec. II.C in Ref. [66] for details) in the following form [67]

$$\frac{\Theta^{\mathrm{S}}}{\Theta_{00}} = \frac{1}{2}\left[v^2(3\dot{X}_3\dot{X}_3 - 1) - 6v\frac{\Phi}{\tilde{U}}X'_3\dot{X}_3 - (1-v^2)\frac{\tilde{T}}{\tilde{U}}(3X'_3X'_3 - 1)\right], \tag{A6a}$$

$$\frac{\Theta^{\mathrm{V}}}{\Theta_{00}} = v^2\dot{X}_1\dot{X}_3 - \frac{\tilde{T}}{\tilde{U}}(1-v^2)X'_1X'_3 - v\frac{\Phi}{\tilde{U}}(X'_1\dot{X}_3 + \dot{X}_1X'_3), \tag{A6b}$$

$$\frac{\Theta^{\mathrm{T}}}{\Theta_{00}} = v^2\dot{X}_1\dot{X}_2 - \frac{\tilde{T}}{\tilde{U}}(1-v^2)X'_1X'_2 - v\frac{\Phi}{\tilde{U}}(X'_1\dot{X}_2 + \dot{X}_1X'_2), \tag{A6c}$$

where

$$\Theta_{00} = \frac{\mu_0\tilde{U}}{\sqrt{1-v^2}}\frac{\sin(\frac{1}{2}kX'_3\xi_{\mathrm{C}})}{\frac{1}{2}kX'_3}\cos(\boldsymbol{k}\cdot\boldsymbol{x}_0 + k\dot{X}_3v\tau). \tag{A7}$$

By expressing the contributions of individual string segments in terms of currents (A6), one can perform summations across all segments to derive the complete stress-energy tensor for the cosmic string network under consideration. The string segments undergoing decay simultaneously are combined into what is referred to as "consolidated string segments" [51], as outlined in detail in Sec. III.A. of Ref. [66].

Incorporating all the modifications into the CMBACT code, we can now make predictions for the CMB anisotropies arising from current-carrying cosmic strings. One should notice that there is no assumption about scaling behavior of the network. Therefore, we can apply this algorithm to a "frozen" network that might occur as a solution $v \propto \frac{\xi_c}{\tau} \propto \sqrt{1-Y} \propto \tau^{-s}$ as well as to the single-parameter scaling model to which we now turn. References [31,32] discuss these solutions in detail.

For a detailed comparison of the CMB anisotropies originating from NG and current-carrying cosmic strings, we present figures that depict the separations for scalar, vector, and tensor modes for BB, TT, EE, and TE components. Specifically, our analyses includes various values of Y_{sc}, a parameter governing the charge value during the radiation-dominated period, as detailed in Sec. III and illustrated in Fig. 14.

Additionally, we extend our calculations to explore alternative scenarios. In Fig. 16, we show the results of CMB anisotropies generated by cosmic string networks with currents, exhibiting linear scaling regimes denoted as (b) and (d) models, as described in Sec. III B. Furthermore, Fig. 15 presents the CMB anisotropies stemming from cosmic string networks undergoing the "frozen" regime during the radiation-dominated epoch, characterized as (a) and (c) models, and described in Sec. III B.

Analysing Fig. 14 one sees that, starting from the NG limit ($Y_{\mathrm{SC}} = 0$) scalar modes have a slight increase until $Y_{\mathrm{SC}} \approx 0.3$, then decrease until $Y_{\mathrm{SC}} \approx 0.7$ and finally drastically increase for $Y_{\mathrm{SC}} > 0.7$. The vector and tensor modes in general have monotonic decreases with increasing values of Y_{SC}. For large multipole moments (small angular scales) $\ell \gtrsim 200$ for vector modes we also see that after some threshold, the relevant contribution increases.

This enhancement of scalar modes and decrease of vector and tensor modes can be explained from the point of view of the string network evolution. Specifically, the reason stems from the fact that with an increase of the

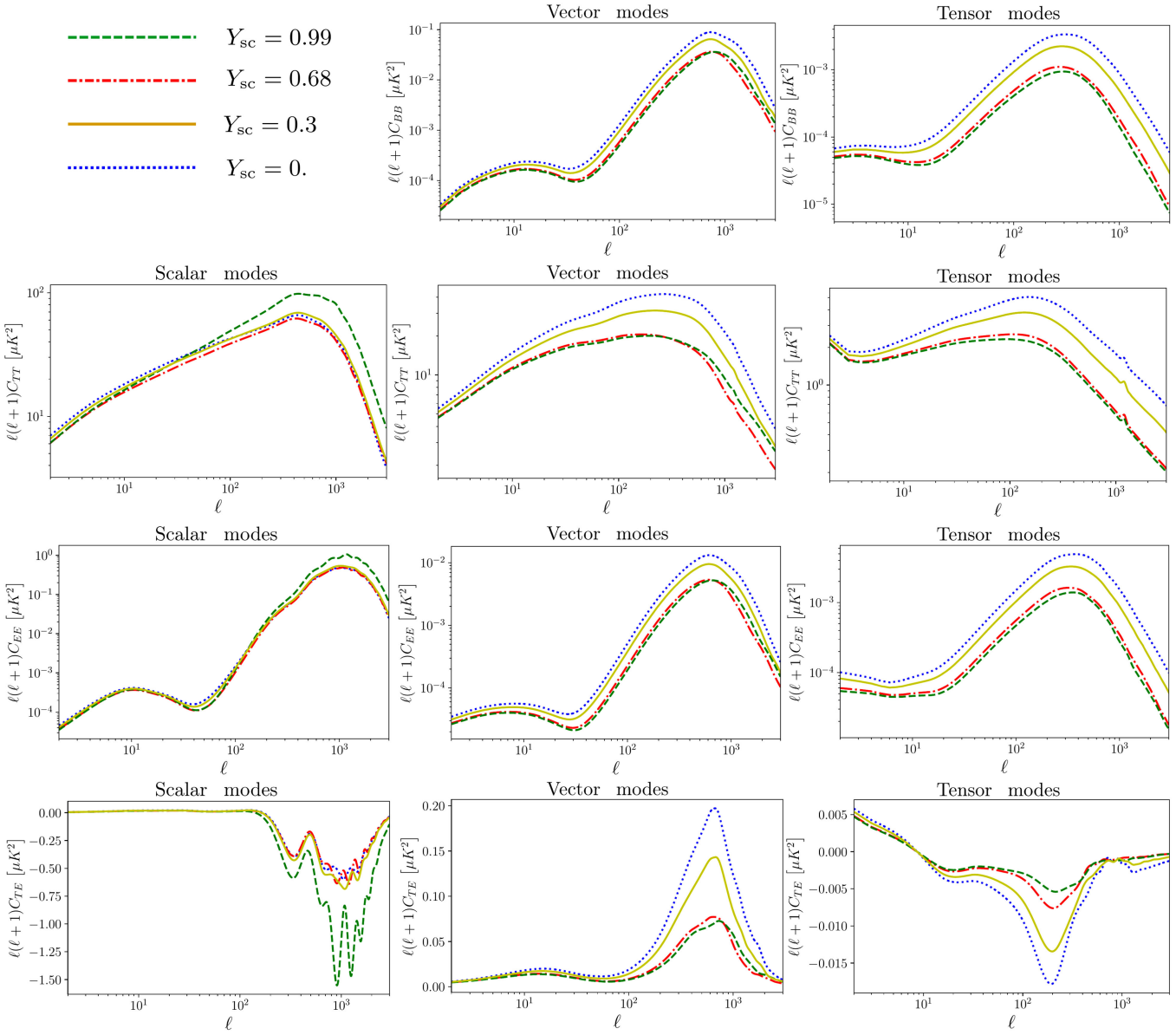

FIG. 14. The BB, TT, EE, and TE components of the CMB anisotropies induced by current-carrying cosmic strings evolving according to Eqs. (12) are examined with varying values of Y_{SC}.

charge on cosmic strings, the rms velocity decreases. This decrease of the velocity leads to the decrease of the vector and tensor modes. At the same time, with smaller velocity the string network loses comparatively less energy and therefore becomes more dense, and a denser string network results in enhanced scalar modes, which we also see for the (b) and (d) models in Fig. 16.

The peak enhancement of scalar modes for current-carrying strings occurs when the network is in a frozen state ($Y_{SC} = 1$). In both the (a) and (c) cases, the contribution from scalar modes significantly surpasses that of standard NG strings, as illustrated in the left column of Fig. 15. Simultaneously, the vector and tensor modes experience substantial suppression, as evident in the second and third columns of panels in Fig. 15. Notably, for small angular scales ($\ell > 1000$), the vector modes of a frozen network dominate over the NG case. These distinctive features have the potential to serve as discriminators between ordinary cosmic strings and those involving current-carrying strings.

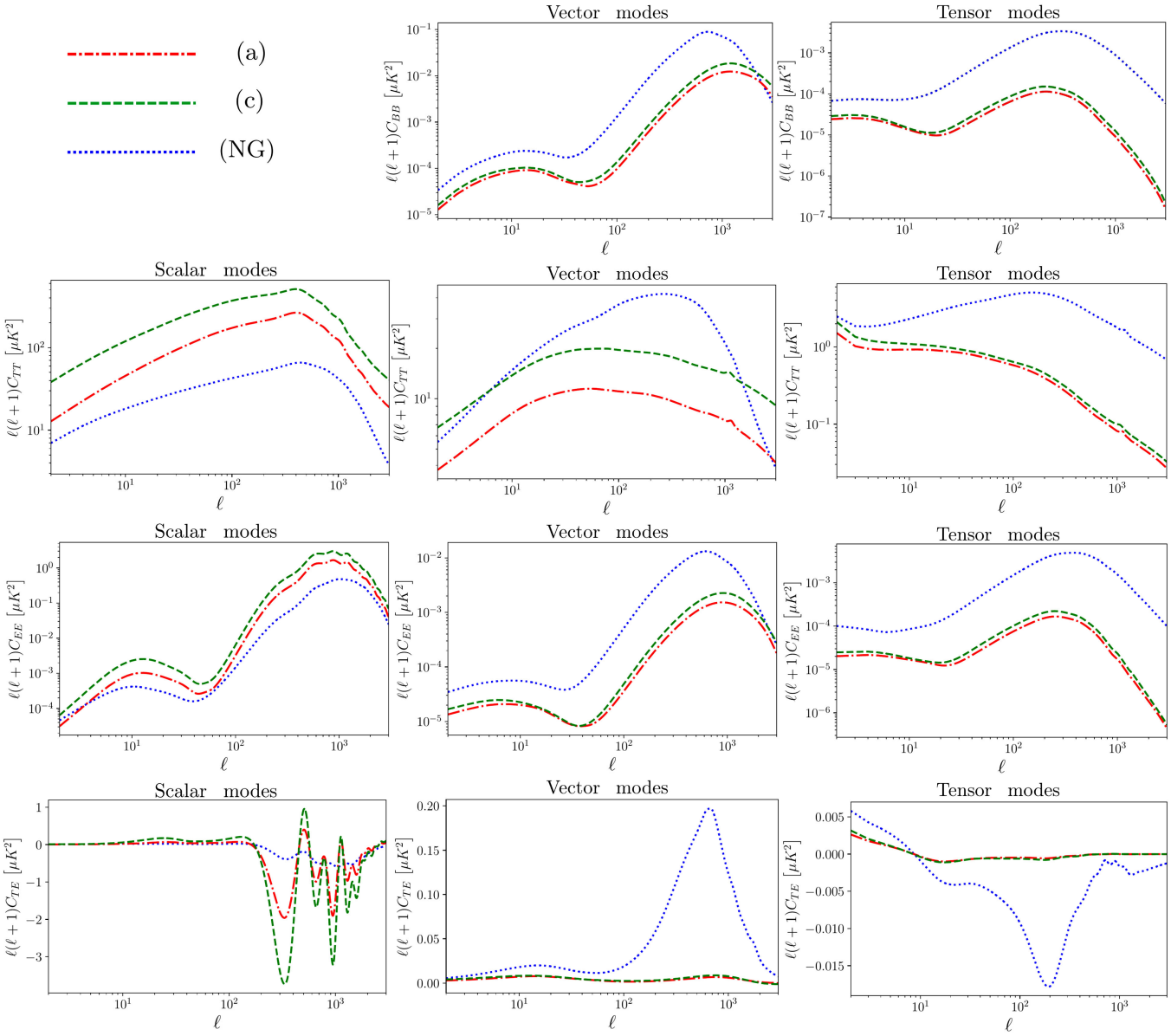

FIG. 15. CMB anisotropies arising from standard (NG) and current-carrying "frozen" cosmic string networks are investigated. The parameters align with the models (a) and (c) outlined in Sec. III B and Ref. [31].

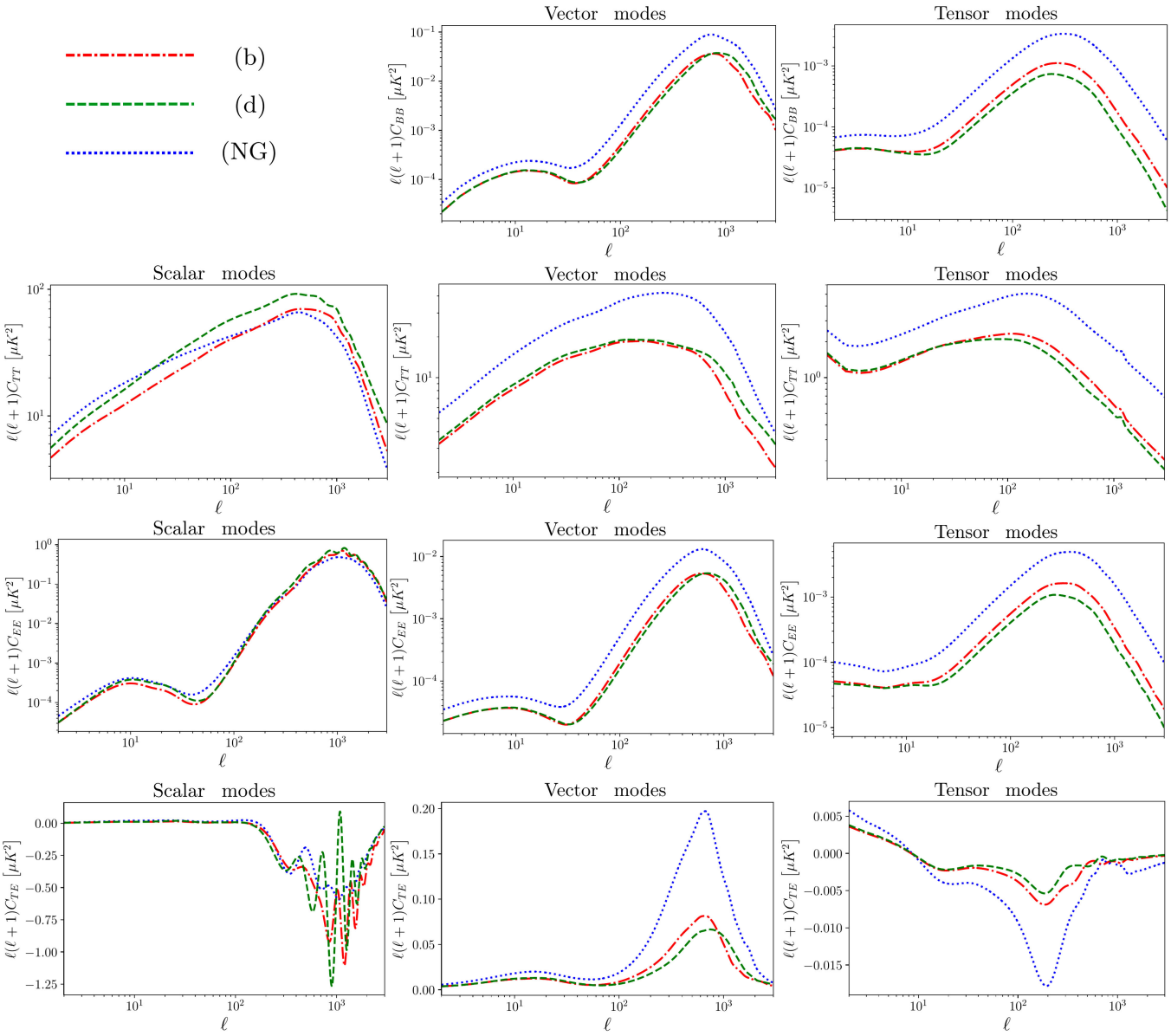

FIG. 16. CMB anisotropies originating from standard (NG) and current-carrying cosmic strings with the linear scaling regime are examined. The parameters are in accordance with the models (b) and (d) detailed in Sec. III B and Ref. [31].

[1] R. Jeannerot, J. Rocher, and M. Sakellariadou, Phys. Rev. D **68**, 103514 (2003).
[2] S. Sarangi and S.-H. H. Tye, Phys. Lett. B **536**, 185 (2002).
[3] E. Allys, J. Cosmol. Astropart. Phys. 04 (2016) 009.
[4] M. Yamada and K. Yonekura, Phys. Rev. D **106**, 123515 (2022).
[5] E. Witten, Nucl. Phys. **B249**, 557 (1985).
[6] A.-C. Davis and P. Peter, Phys. Lett. B **358**, 197 (1995).
[7] G. Lazarides and Q. Shafi, Phys. Lett. **151B**, 123 (1985).
[8] P. Peter, Phys. Rev. D **49**, 5052 (1994).
[9] J. Garaud and M. S. Volkov, Nucl. Phys. **B826**, 174 (2010).
[10] Y. Abe, Y. Hamada, and K. Yoshioka, J. High Energy Phys. 06 (2021) 172.
[11] E. J. Copeland, R. C. Myers, and J. Polchinski, J. High Energy Phys. 06 (2004) 013.
[12] E. J. Copeland and T. W. B. Kibble, Proc. R. Soc. A **466**, 623 (2010).
[13] M. F. Oliveira, A. Avgoustidis, and C. J. A. P. Martins, Phys. Rev. D **85**, 083515 (2012).

[14] C. J. A. P. Martins, E. P. S. Shellard, and J. P. P. Vieira, Phys. Rev. D **90**, 043518 (2014).
[15] J. P. P. Vieira, C. J. A. P. Martins, and E. P. S. Shellard, Phys. Rev. D **94**, 096005 (2016).
[16] A. Pourtsidou, A. Avgoustidis, E. J. Copeland, L. Pogosian, and D. A. Steer, Phys. Rev. D **83**, 063525 (2011).
[17] I. Y. Rybak, A. Avgoustidis, and C. J. A. P. Martins, Phys. Rev. D **99**, 063516 (2019).
[18] J. R. C. C. C. Correia and C. J. A. P. Martins, Phys. Rev. D **106**, 043521 (2022).
[19] L. Sousa and P. P. Avelino, Phys. Rev. D **94**, 063529 (2016).
[20] T. Charnock, A. Avgoustidis, E. J. Copeland, and A. Moss, Phys. Rev. D **93**, 123503 (2016).
[21] P. Auclair, P. Peter, C. Ringeval, and D. Steer, J. Cosmol. Astropart. Phys. 03 (2021) 098.
[22] P. Auclair, S. Blasi, V. Brdar, and K. Schmitz, J. Cosmol. Astropart. Phys. 04 (2023) 009.
[23] I. Rybak and L. Sousa, J. Cosmol. Astropart. Phys. 11 (2022) 024.
[24] A. Drew and E. P. S. Shellard, Phys. Rev. D **105**, 063517 (2022).
[25] J. R. C. C. C. Correia and C. J. A. P. Martins, Phys. Rev. D **104**, 063511 (2021).
[26] A. Drew and E. P. S. Shellard, Phys. Rev. D **107**, 043507 (2023).
[27] C. J. A. P. Martins and E. P. S. Shellard, Phys. Rev. D **73**, 043515 (2006).
[28] C. Ringeval, M. Sakellariadou, and F. R. Bouchet, J. Cosmol. Astropart. Phys. 02 (2007) 023.
[29] J. J. Blanco-Pillado, K. D. Olum, and B. Shlaer, Phys. Rev. D **83**, 083514 (2011).
[30] C. J. A. P. Martins, P. Peter, I. Y. Rybak, and E. P. S. Shellard, Phys. Rev. D **103**, 043538 (2021).
[31] C. J. A. P. Martins, P. Peter, I. Y. Rybak, and E. P. S. Shellard, Phys. Rev. D **104**, 103506 (2021).
[32] I. Y. Rybak, C. J. A. P. Martins, P. Peter, and E. P. S. Shellard, Phys. Rev. D **107**, 123514 (2023).
[33] C. J. A. P. Martins and E. P. S. Shellard, Phys. Rev. D **54**, 2535 (1996).
[34] C. J. A. P. Martins and E. P. S. Shellard, Phys. Rev. D **65**, 043514 (2002).
[35] N. Bevis, M. Hindmarsh, M. Kunz, and J. Urrestilla, Phys. Rev. D **75**, 065015 (2007).
[36] C. Ringeval, Adv. Astron. **2010**, 380507 (2010).
[37] I. Y. Rybak and L. Sousa, Phys. Rev. D **104**, 023507 (2021).
[38] B. Rudak and M. Panek, Phys. Lett. B **199**, 346 (1987).
[39] B. Cyr, J. Chluba, and S. K. Acharya, Mon. Not. R. Astron. Soc. **525**, 2632 (2023).
[40] B. Cyr, J. Chluba, and S. K. Acharya, Phys. Rev. D **109**, L121301 (2024).
[41] M. Sazhin and M. Khlopov, Sov. Astron. **33**, 98 (1989).
[42] O. S. Sazhina, D. Scognamiglio, M. V. Sazhin, and M. Capaccioli, Mon. Not. R. Astron. Soc. **485**, 1876 (2019).
[43] K. Benabed and F. Bernardeau, Phys. Rev. D **61**, 123510 (2000).
[44] J. Lizarraga, J. Urrestilla, D. Daverio, M. Hindmarsh, and M. Kunz, J. Cosmol. Astropart. Phys. 10 (2016) 042.
[45] A. Lazanu and E. P. S. Shellard, J. Cosmol. Astropart. Phys. 02 (2015) 024.
[46] A. Lazanu, E. P. S. Shellard, and M. Landriau, Phys. Rev. D **91**, 083519 (2015).
[47] R. A. Battye and S. J. Cotterill, Phys. Rev. Lett. **127**, 241601 (2021).
[48] R. A. Battye, S. J. Cotterill, and J. A. Pearson, J. High Energy Phys. 04 (2022) 005.
[49] K. Fujikura, S. Li, and M. Yamaguchi, J. High Energy Phys. 12 (2023) 115.
[50] T. Hiramatsu, M. Lilley, and D. Yamauchi, arXiv:2312.16091.
[51] L. Pogosian and T. Vachaspati, Phys. Rev. D **60**, 083504 (1999).
[52] N. Aghanim *et al.* (Planck Collaboration), Astron. Astrophys. **641**, A6 (2020); **652**, C4(E) (2021).
[53] Planck Collaboration XXV, Astron. Astrophys. **571**, A25 (2014).
[54] P. Peter, Phys. Rev. D **45**, 1091 (1992).
[55] Y. Abe, Y. Hamada, K. Saji, and K. Yoshioka, J. High Energy Phys. 02 (2023) 004.
[56] S. Barr and A. Matheson, Phys. Lett. B **198**, 146 (1987).
[57] V. F. Mukhanov, H. A. Feldman, and R. H. Brandenberger, Phys. Rep. **215**, 203 (1992).
[58] A. Stebbins, S. Veeraraghavan, R. H. Brandenberger, J. Silk, and N. Turok, Astrophys. J. **322**, 1 (1987).
[59] D. C. N. da Cunha, J. Harnois-Deraps, R. Brandenberger, A. Amara, and A. Refregier, Phys. Rev. D **98**, 083015 (2018).
[60] H. Jiao, R. Brandenberger, and A. Refregier, Phys. Rev. D **108**, 043510 (2023).
[61] B. Cyr, H. Jiao, and R. Brandenberger, Mon. Not. R. Astron. Soc. **517**, 2221 (2022).
[62] A. A. Fraisse, C. Ringeval, D. N. Spergel, and F. R. Bouchet, Phys. Rev. D **78**, 043535 (2008).
[63] L. Pogosian, S.-H. H. Tye, I. Wasserman, and M. Wyman, J. Cosmol. Astropart. Phys. 02 (2009) 013.
[64] T. Vachaspati, Phys. Lett. B **265**, 258 (1991).
[65] F. Ferrer, H. Mathur, T. Vachaspati, and G. Starkman, Phys. Rev. D **74**, 025012 (2006).
[66] A. Albrecht, R. A. Battye, and J. Robinson, Phys. Rev. D **59**, 023508 (1998).
[67] I. Y. Rybak, A. Avgoustidis, and C. J. A. P. Martins, Phys. Rev. D **96**, 103535 (2017).